ISSN: 2767-0171

ablation, and others [4,5]. Particularly interest concerns the preparation of carbon nanoparticles (CNPs) and carbon-dots (CDs) using laser beams [6].

High intensity lasers operating from UV to visible and IR, using continuum wave (CW) and pulsed waves can be focused on to carbon targets to produce effects of atoms, molecules and clusters removing. The irradiation can be performed in solids placed in a vacuum, air, gases, and liquids.

The laser ablation of solid targets placed in liquids is employed as a promising method to produce controllable nanoparticles of different size and shape, as a function of the laser properties and of the irradiation conditions [7]. This method generates a vaporization at the solid-liquid interface with bubble formation within which atoms and molecules collides generating nanostructures released in the liquid at the bubble explosion phase. The interest for this method of nanoparticle preparation comes from its simple setup, controllable dispersion concentration, economical and reproducible technique, and use of low-cost laser sources.

The size of the nanoparticles and their distribution depends on many parameters, such as the conditions of laser irradiation, energy released to the target, used wavelength and intensity, type of liquid used [8]. The nature of the liquid in which the target is immersed is fundamental for the generation of functionalized nanoparticles [9].

Not only ns pulsed lasers, but also CW lasers can be used to generate small nanoparticles of the order of 1-10 nm, called C-dots, having the characteristic to be luminescent in the visible region under the excitation of energetic radiations, such as X-rays and UV ones. Recently, it has been discovered that also low energetic diode lasers with long pulse duration (ms) may ablate carbon targets producing CDs [10].

This investigation would present the possibility to realize CDs in a Phosphate-buffered saline (PBS) solution, with a pH ~ 7.4, commonly used in biological research, by using a CW laser diode emitting photons at 450 nm wavelength with an output intensity of 50 Watt. The irradiated target was a green based material realized using a porous vegetal carbon. The C-dots possess high blue luminescence which has been induced by UV excitation. Due to their high biocompatibility, minimum cytotoxicity, ultra-light weight, ability to enter in cells by spontaneous mechanism due to their small size, possibility to be functionalized with different chemical groups, CDs found a vast area of interest in Biology, Medicine, microelectronics, matter physics and other fields. In fact, CDs can be used as drug delivery, bioimaging, biosensors, scaffolds in tissue engineering, cancer therapy, gene therapy, immune therapy, different types of biomedical imaging, Raman imaging, biosensors, tissue engineering, innovative polymer preparation, and others.

EXPERIMENTAL SECTION

A GaAs laser diode system operating at 450 nm wavelength (blue), in CW, 50 W output power, 1 mm^2 spot diameter, with an intensity of $5x10^3$ W/s cm^2 has been employed to irradiate the carbon target with an incidence angle of 0°.

Vegetable carbon (Charcoal) was used as a target. Coal is a common fuel produced by the wood carbonization process and consists of the transformation of an organic compound into a carbonaceous material, a process that occurs during the burning of combustible wood, and which occurs at high temperatures in the presence of a very low concentration of oxygen (oxidizing agent) [11].

The charcoal composition depends on many factors, such as the method of preparation, type of wood burned, content of water and functional groups of oxygen and other substances, geographic area, temperature, and others. The composition may change also by the different methods of preparation which may use different temperatures, oxygen concentrations or other gases, time of treatment, environment humidity, and other factors. Charcoal is a green material and contains varying amounts of hydrogen and oxygen as well as ash and other impurities that, together with the structure, determine their final properties. The approximate composition of charcoal can be taken from the literature that reports the following values expressed in wt % of average concentrations [12,13]: C = 66.9%: H = 4.4%; O = 7.6 %; N = 1.3 %; S = 1.1%; Moisture = 7.2%; Ash = 11.5%; Cl = 0.1%.

Charcoal contains many functional oxygen groups, such as carbonyl (C=O), carboxyl (O=C-OH), epoxide (-C-O-C-), hydroxyl (-OH), H_2O, CO_2, N_2, and other gases.

Charcoal as an amorphous carbon structure, is strongly porose with a porosity of the order of 65%-75%, and many micrometric pores. This produces a low-density property, below 1 g/cm^3, generally around 0.5 g/cm^3 [14]. It has very high absorbance of many gases and liquids, such as water and biological liquids, high hydrophilicity, high absorbance of visible light, and appears black colored, contains micrometric particle inside the pores, has very low reactivity having a pH near neutral

ISSN: 2767-0171

[15]. Its thermal and electrical conductivity are low, of the order of 0.2 W/mK and 10^{-2} S/m, respectively [16,17]. Thus, it is a good thermal and electrical insulator and, from the point of view of the electrical conductivity, it is about four orders of magnitude lower than in graphite.

Charcoal has low hardness, mechanical resistance, and elasticity; the dynamical hardness is of the order of 20 MPa [18].

The CW bleu laser irradiation was performed in a solution containing deionized water and 10 X Phosphate-Buffered Saline (PBS) solution. This last is a 10-fold concentrated blend of phosphate buffer and saline solution with a pH = 7.4 and RNase-free, typically used in molecular Biology [19].

The PBS solution was prepared by dissolving a 2 g PBS tablet, purchased by Sigma Aldrich [20], in a distilled water volume of 200 ml.

The CW laser irradiation was produced in air, at room temperature (20°C), 1 atm pressure, and 50% humidity. The laser is focused on a vegetable carbon target (charcoal) placed in the PBS solution. This carbon sample has a parallelepiped shape, 2 cm^2 surface, 1 mm thickness and a pristine mass of about 0.12 g, corresponding to a density of 0.6 g/cm^3. The C target is placed in a glass beaker containing 4 cm^3 PBS solution. The positioning of the target in the PBS represents an important phase for the correct ablation and CDs generation. The C-target is first immersed in the PBS to absorb the maximum liquid from the solution, so that left free to float a thin layer of liquid is generated on its surface that will be laser irradiated. This liquid allows the drainage of nanoparticles and CDs generated by the laser ablation process towards the PBS solution where they will be suspended.

The laser irradiation occurs on the floating target for times from 30 min up to 2 hrs. The used experimental setup is schematized in Figure 1a, and the setup photo is reported in Figure 1b. The ablation crater produced by the laser ablation after 30 min irradiation time is reported in Figure 1c, while the aspect of the final solution in the beaker after 2 hr irradiation time in Figure 1d.

The pristine solution of PBS, without the carbon target, was laser irradiated for 1 hr at the same conditions adopted for the irradiation of the vegetable carbon in PBS to demonstrate that it does not give luminescence and formation of carbon nanoparticles. Moreover, the same laser ablation of charcoal was also performed in distilled water to demonstrate that it does not produces CDs but only C nanoparticles without any luminescence effect.

ISSN: 2767-0171

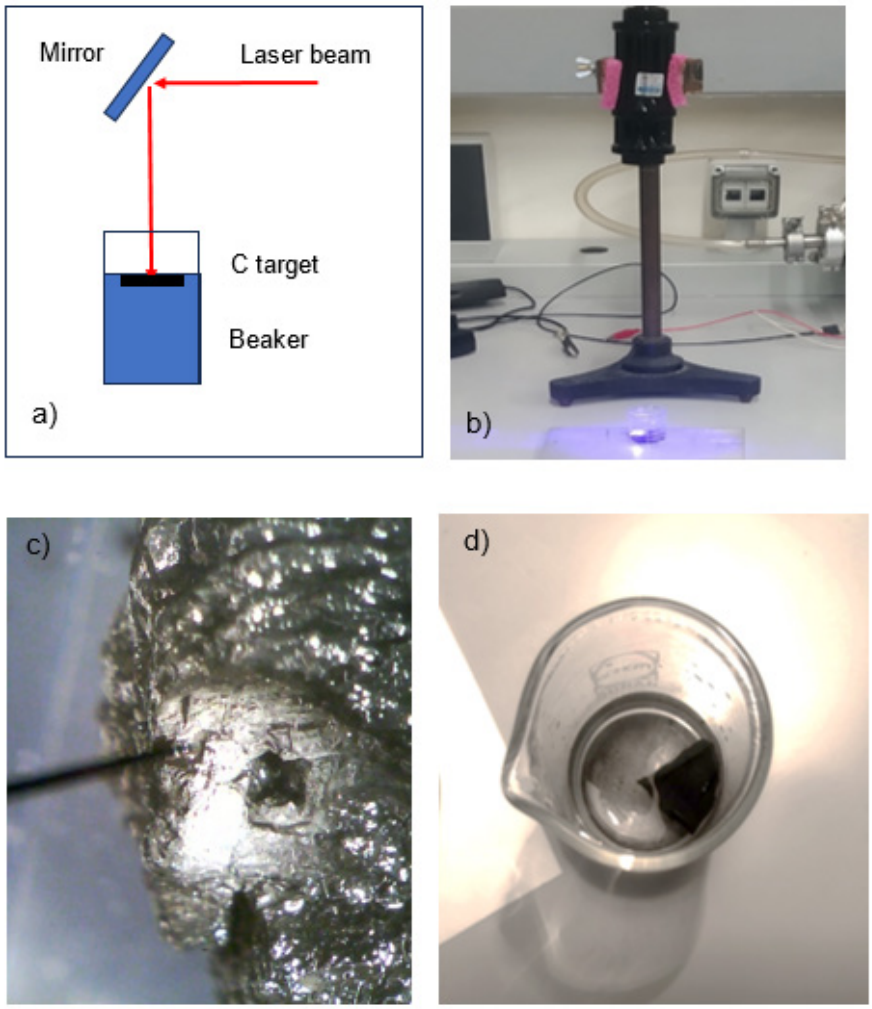

Figure 1. Scheme of the experimental setup (a) and its photo (b), crater produced in the carbon at 30 min irradiation time (c) and final solution after 1 hr irradiation time (d).

Measurements of crater geometry and ablation yield, in terms of removed mass per minute, were carried out with accuracy.

The attenuated total reflectance coupled to the Fourier transform infrared spectroscopy (ATR-FTIR), have been acquired using the spectrophotometer JASCO Mod. 4600 operating in the (400-4000) cm^{-1} wavenumber region, with a minimal resolution of about 0.7 cm^{-1}.

UV-Vis measurements have been performed using the spectrophotometer Jasco Mod. V-750 with double beam to evaluate the absorbance and transmittance of the prepared CDs dispersion in the PBS solution in the (250–800) nm wavelength range, using transparent quartz cuvettes.

The optical spectrometer Avantes AvaSpec-2048-USB2 coupled to optical fiber input was employed for measurements of the luminescence in the region 200-800 nm of the prepared suspension containing the CDs. The luminescence was investigated exciting the dispersion with an UV light source operating at 365 nm. The UV lamp has a fluence of about 100 mJ/cm^2 at 10 cm distance.

RESULTS AND DISCUSSION

The analyses relative to the crater produced by the laser ablation (see Figure 1c) demonstrated that in 30 minutes of continuum irradiation is produced a crater volume of about 1.8 mm^3. Assuming the vegetal carbon density of 0.6 g/cm^3, as experimentally measured, the removed carbon mass in 30 minutes irradiation time was about 1.1 mg. Thus, the measured ablation yield is of about 36 μg/min, corresponding to a number of ablated atoms per minute of $1.8x10^{17}$ C atoms.

Assuming the CDs to have a spherical shape with 1 nm radius and the density of the amorphous carbon of 2.44 g/cm^3, their

DOI: https://doi.org/10.35702/nano.10014

ISSN: 2767-0171

mass corresponds to about $1.02x10^{-20}$ g. Thus, the ablation yield would correspond to a production of approx. $3.5x10^{15}$ CDs/min. However, some micrometric particles are also produced by the laser ablation and probably also C nanoparticles bigger than 10 nm could be produced, thus it is reasonable to expect that only 10% or less of the ablated carbon goes to form CDs, decreasing their production at a value of about $3.5x10^{14}$ CDs per minute, or a little less. A confirmation of this percentage was given by the measure of the residual mass of the micrometric particles obtained by the liquid filtering process through micromembranes.

The vegetable carbon used as a target has been submitted to ATR-FTIR spectroscopy to have information on the oxygen functional groups present in its structure, responsible of high IR absorption. Figure 2 reports the ATR-FTIR spectrum relative to the vegetal carbon used as a laser irradiation target.

Such a spectrum confirms that different oxygen functional groups are present in the carbon sample. Here are evident the hydroxyl (-OH), carboxylic (C=O), carbonylic (O=C-OH), epoxydic (-C-O-C), carbon nitride (C-N) and other groups. The matrix also contains water, and diffused gases, such as hydrogen, oxygen, and nitrogen.

The transmittance is high and in the wavenumber region higher than 2000 cm^{-1} the average transmittance is of about 98 %, except for the strong absorbent peaks due to the C=C at 1542 cm^{-1}, and the C=N, C=O, -C-O-C, C-N and C-O peaks in the region 2200-1320 cm^{-1}, in agreement with the literature [6,21].

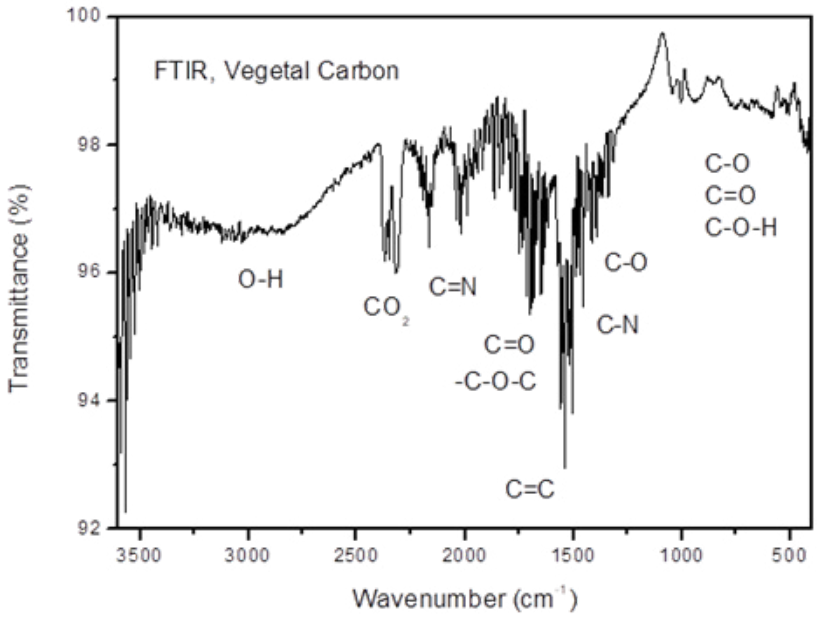

Figure 2. ATR-FTIR spectrum of the vegetal carbon target.

The high photon intensity released by the CW laser to the target irradiation of the vegetable carbon produces different phenomena, such as heating inside the crater volume, single and multiple photon absorption, radical generation, atomic and molecular detachment, carbon atom collisions and nucleation, and others. Multiple photon absorption enhances the electron energy transferring it from the valence band to the conduction one, generating ionization processes, free radicals and breaking of chemical bonds, molecular scissions and removing of weakly bonded carbon molecules [22].

Such processes generate carbon nanoparticles in the PBS solution (from nm to micrometric sizes) and nanometric CDs, which can be detected by their visible luminescence under UV excitation lamp, in agreement with previous experiments reported in the literature [6,10,22,23].

The CDs in the PBS solution have been investigated using as an exciting source a UV lamp centered at 365 nm wavelength, having about 10 nm full-width-of-half-maximum (FWHM), and detecting the visible luminescence trough a fiber (300 nm diameter) transporting the light to the Avantes

ISSN: 2767-0171

spectrophotometer operating in the region 200-800 nm. The CDs suspension appears transparent to the white visible light and blue-colored under UV irradiation. Fig. 3 shows a photo of the solution under visible light (a) and under UV light irradiation (b).

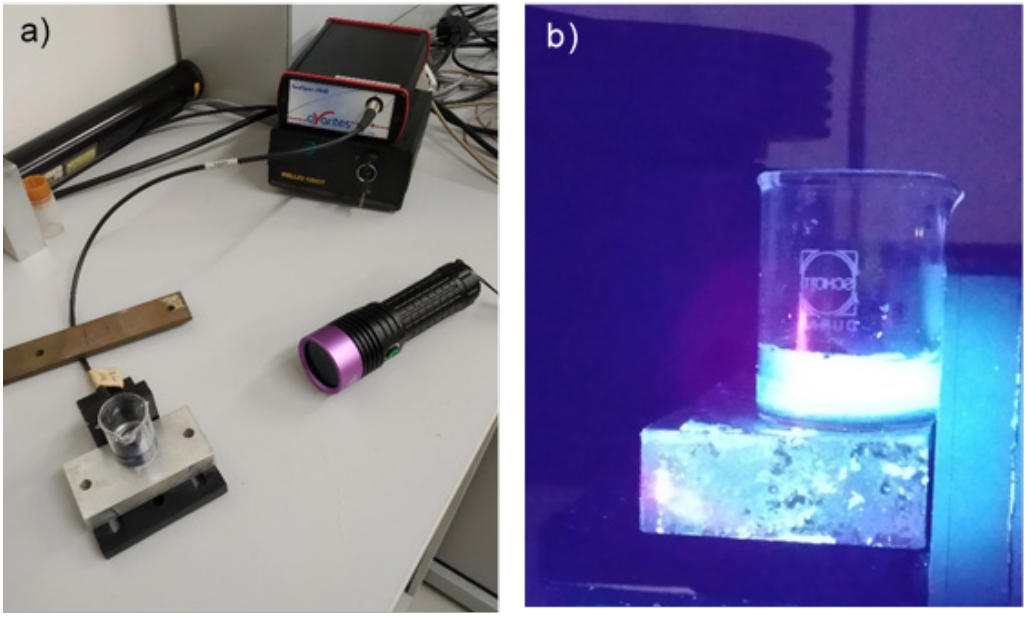

Figure 3. Set up for CDs luminescence induced by UV lamp (a) and blue light suspension emission under UV irradiation (b).

Figure 4 shows a spectra comparison between the UV lamp emission (a), the background emission of the cuvette containing only the PBA solution under UV irradiation (b), the luminescence emitted from the CDs suspension in PBS under UV excitation produced by 45 min (c) and 2 hr laser irradiation time (d).

The CDs luminescence induced by UV excitation growths with their concentration, i.e. with the laser irradiation time of the vegetable carbon target in PBS solution. It shows a significant peak at 474 nm wavelength (blue color) and two minor lateral peaks at about 450 nm and 520 nm. The central emission at 474 nm has a width (FWHM) of about ±10 nm.

The CDs luminescence peaks induced by UV is well reproducible and grows about linearly with the CDs concentration, i.e. with the CW laser irradiation time of the vegetal carbon target in PBS.

The UV photons exciting the CDs luminesce have 3.39 eV energy, while the luminescence emits photons at 2.61 eV energy. Such data indicate that the UV photons are absorbed by molecular electrons in valence band, that acquire sufficient energy to pass into the conduction band. Here, in a time less than 10^{-12} s decay spontaneously in the valence band or in states of surface levels generated above the valence band, as defects and intermediate level traps, emitting characteristic luminescent photons [24].

Literature reports that the CDs luminescence can be due to three phenomena: surface state, carbon core state, and molecular state [24].

The surface state is due to the surface functional oxygen groups connecting with the carbon backbone, which control the electron structures and energy level by hybridization. The luminescence can be adjusted by altering types and contents of surface functional groups or the heteroatoms doping.

The carbon core state refers to the π–π^* electron transitions of the conjugated sp2 domains. The size of the isolated sp2 subdomain determines the light emission luminescence of CDs15.

The molecule state refers to the molecular fluorophores or their aggregates, which are connected with CDs dominated by the fluorescence, and it generally endows CDs with a strong photoluminescence and a high photoluminescence quantum yield, referred to the number of emitted photons per absorbed photon.

DOI: https://doi.org/10.35702/nano.10014

ISSN: 2767-0171

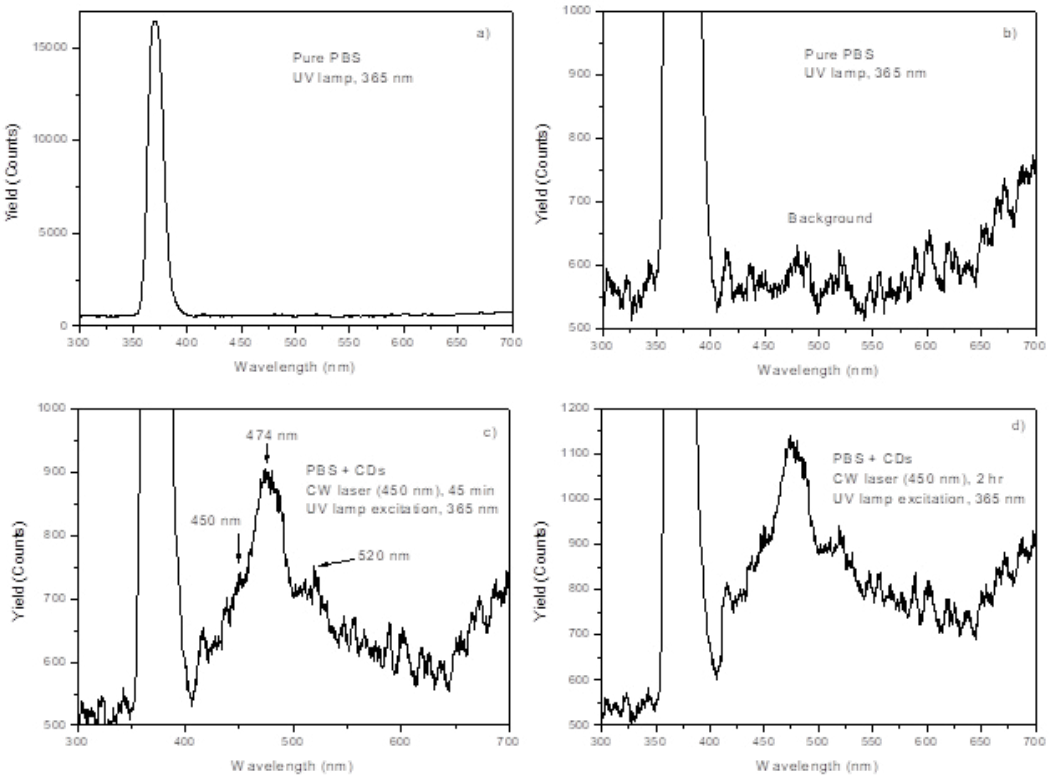

Figure 4. Comparison between the UV lamp emission (a), the background coming from the pure PBS under UV excitation (b) and the CDs luminescence produced by 30 min (c) and 1 hr (d) laser irradiation time.

The CDs luminescence induced by 365 nm UV lamp grows with the laser irradiation time of the target. The plot comparison reported in Fig. 5a shows a very good proportionality between the laser irradiation time and the CDs luminescence yield in the (400-600) nm wavelength region. Fig. 5b reports the plot of the luminescence intensity (counts) at 474 nm versus the CW laser irradiation time of the carbon target with experimental errors of the order of 4%. The light yield is well proportional to the laser irradiation time, i.e. to the CDs concentration in the PBS liquid.

ISSN: 2767-0171

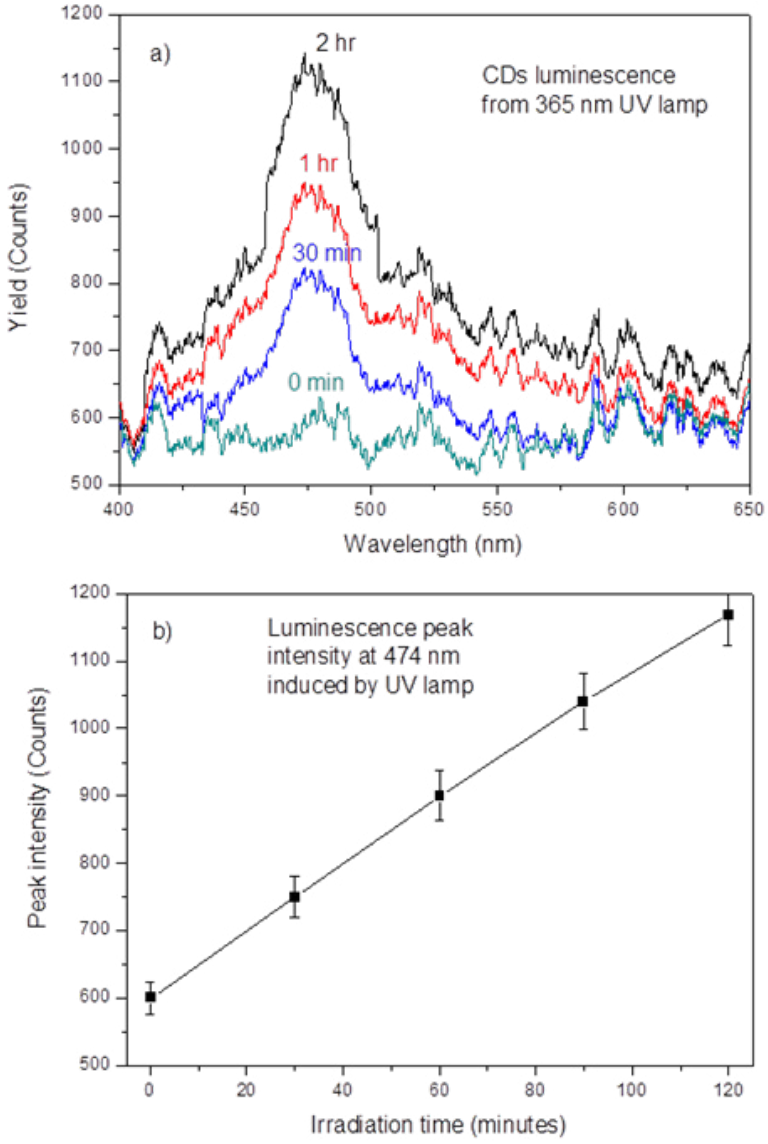

Figure 5. CDs luminescence spectra induced by 365 nm UV lamp versus wavelength and CW laser irradiation (a) and luminescence intensity linearity with the CW laser irradiation time (b).

The absorbance measurements have been done using the UV-Vis spectroscopy in the region 250-700 nm wavelength both on the PBS pure solution and in the CDs suspension in PBS solution contained in quartz cuvettes.

Figure 6 shows the result of the absorbance measurements in the CDs suspension in PBS, at 30 min, 60 min and 120 min CW laser irradiation of the vegetable carbon target. The absorbance spectra show a low absorbance in the visible region 400-800 nm, where the suspension is transparent, and a significant absorbance in the near UV region 250-350 nm. The absorbance decreases exponentially going form about 250 nm up to 400 nm, showing some discontinuity at about 362 nm, due to nanometric structures highly absorbent the UV radiation, according to the literature [25,26].

DOI: https://doi.org/10.35702/nano.10014

ISSN: 2767-0171

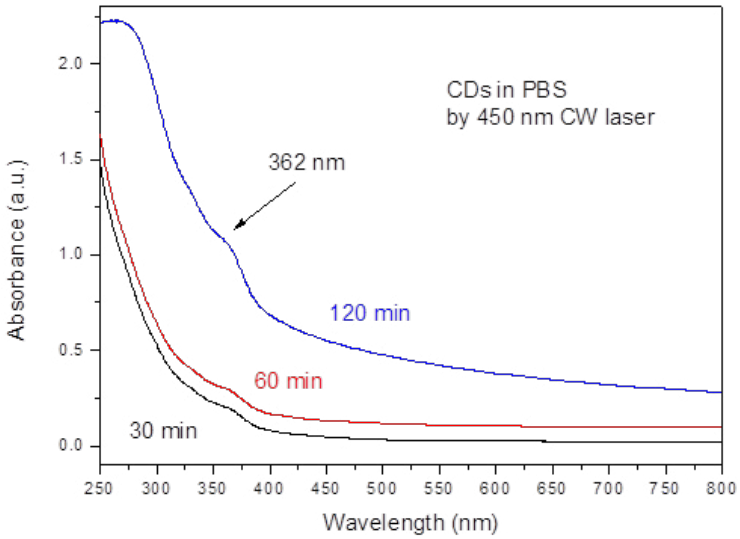

Figure 6. UV-Vis Absorbance (a) of the CDs suspension in PBS, at 30 min and 60 min CW laser irradiation of the carbon target versus the wavelength.

In agreement with the literature [27,28], the CDs suspension in PBS absorbance has a trend decreasing exponentially from short wavelengths (~ 250 nm) to about 500 nm, and a near constant absorbance very low in the region 500 nm-800 nm.

Molecular electronic transitions take place when electrons in a molecule are excited from one energy level to a higher energy level that can be determined by UV-Vis spectroscopy. In carbon molecules, the promotion of an electron from a π orbital to an antibonding π* orbital is denoted as a $\pi \rightarrow \pi^*$ transition. The absorbance discontinuity at about 362 nm may be due to $\pi \rightarrow \pi^*$ transitions involving the aromatic C=C sp2 carbon bonds, and the C=O chemical bonds. Such transitions correspond to double bonding electron oscillation along the bond axis. However also the $n \rightarrow \pi^*$ transitions may occur as result of the lone-pairs vibrating out of plain, due to surface level states above the valence band form which the transition with the conduction bans may occurs [29].

Some literature reports that the shoulder at 362 nm in the UV-vis spectroscopy may be due to the existence of $n \rightarrow \pi^*$ transition of C=C and C=O bonds [30]. The carbonyl groups are assumed to be formed on the surface of CDs during the carbon nucleation under laser ablation and C=C due to the graphitic type of structure [28,29,31].

According to the literature, the CDs in liquids with a larger diameter (~ 10 nm) generally emit a larger wavelength, with colors such as orange or red, while the CDs with a smaller size (~ 2 nm) emit shorter wavelengths, with colors such as violet or blue [32]. Thus, the blue colored luminescence that we have detected is expected for CDs with a size less than 10 nm but greater than 2 nm, a size which will be investigated using transmission electron microscopy and discussed in the next paper.

Let's now talk about some important applications that the CDs synthesized by us with the laser ablation technique could have.

The luminescence obtained by CDS in suspension in PBS can be employed in many scientific fields. Matter structure physics, radiation dosimetry, microelectronics, sensors, chemistry, biology and medicine, represent some of the fields where it could be specific applications.

CDs can be generated for sensors of metallic ions, such as for Cu^{2+}, Hg^{2+}, and O2- [33-35]. The produced photoluminescence can be employed for the detection of specific molecules in a given sample, for example NO_2 [36], and H_2S [37], and others.

The CDs luminescence may give useful information for medicine and biology because it localizes specific tissues and cell membranes and cytoplasm and depends on the pH value in biological solutions, which may intensify or quenching the luminescence intensity, and may be employed for bioimaging [38].

Moreover, literature reports that carbon nanoparticles and CDs interacting with biological environment may furnish a luminescence depending on the chemical reactions in

DOI: https://doi.org/10.35702/nano.10014

ISSN: 2767-0171

organisms, i.e., on the metabolic phases and could distinguish the metabolism of cancer cells by the healthy cells, giving bioimaging rich in micro-biological information [39,40]. Thus, CDs luminescence bioimaging permits to distinguish functional cells from degenerated ones permitting to discovery damaged cells using nonionizing radiations but only visible or near UV exciting light to induce their bio-luminescence images.

CONCLUSIONS

Vegetal carbon is a green compound with high biocompatibility and possesses peculiar properties in medicine and biology, such as its strong absorbent behaviour towards specific toxins, poisons, and dangerous substances. For example, the vegetable charcoal has the ability to retain on its surface liquids, gases, bacteria, pathogens, toxins and viruses present in the gastrointestinal tract. Carbon nanoparticles and CDs maintain such properties and can be employed to detoxify an organism, to absorb dangerous substances or specific poisons. Carbon nanoparticles and CDs can be used in bioimaging, sensing, and therapy, having low cytotoxicity, high water solubility, high photostability, and tunable excitation wavelength-dependent emission properties and permitting to map the tissues where degeneration and dysfunction occur.

CDs synthesis has been obtained using a CW GaAs diode laser operating at 450 nm irradiating vegetal carbon immersed in a PBS solution at room temperature for different times from 30 min up to 120 min. The long-prolonged irradiation time produces CDs from photo-thermal and photo chemical effects with ejection of carbon atoms and molecules bonded by weak van de Walls forces.

The measured ablation yield is of about $1.8x10^{17}$ C atoms/minute.

Blue coloured CDs luminescence has been obtained by irradiating the CDs with UV radiation at 365 nm wavelength, however, it is expected that also other radiations such as far UV, soft X-rays and energetic electrons may produce such luminescence.

The CDs luminescence was investigated with a sensitive spectrophotometer indicating a good proportionality of the quantum yield with the laser ablation time, i.e. with their concentration in the PBS solution.

UV-Vis spectroscopy has evinced that possible $\pi-\pi^*$ and $n-\pi^*$ transitions may be responsible of the blue observed luminescence that in turn seems to suggest the formation of CDs with sizes less than 10 nm but greater than 2 nm.

Further investigations are in progress to understand the mechanism of CDs formation, to measure the synthetized CDs size and to evince the possibility of using such biocompatible luminescent solutions in the biological field for luminescence in specific cell cultures.

ACKNOWLEDGEMENTS

This work was funded by The European Union-Next Generation EU for the Italian PNRR CAR-BIO-MED CUP J53D23016220001-CI P2022M33MS.

This publication has been also supported by OP RDE, MEYS, Czech Republic, under the project CANAM OP, CZ.02.1.01/0.0/0.0/16_013/0001812 and long-term conceptual development project of the Nuclear Institute of the Czech Academy of Sciences RVO 61389005''. With the support by the Czech Science Foundation (GACR No. 23-06702S).

DECLARATION

ETHICAL APPROVAL

The authors declare that the present study does not involve studies and measurements on humans or animals.

AVAILABILITY OF DATA AND MATERIALS

Data are disponible only on motivated request.

CONFLICT OF INTEREST

The authors declare that they have no conflict of interest.

With the approval of all authors: Lorenzo Torrisi.

REFERENCES

1. Mazura AS, Vovka MA, Tolstoya PM. (2019). Solid-state 13C NMR of carbon nanostructures (milled graphite, graphene, carbon nanotubes, nanodiamonds, fullerenes) in 2000–2019: a mini-review. Proceedings of the 14th International Conference "Advanced Carbon Nanostructures" (ACNS'2019). 28(3):1-13.

2. Torrisi A, Torrisi L, Cutroneo M, Michalcova A, D'Angelo M, Silipigni L. (2023). Ultra-High Molecular Weight Polyethylene Modifications Produced by Carbon Nanotubes and Fe2O3 Nanoparticles. Polymers (Basel). 15(5):1169.

ISSN: 2767-0171

3. Torrisi L, Havranek V, Silipigni L, Torrisi A, Cutroneo M. (2022). Conductive tracks in graphene oxide foils induced by micro beams of MeV helium ions. Diamond and Related materials. 128:109281.

4. Sun Q, Zhang R, Qiu J, Liu R, Xu W. (2018). On-Surface Synthesis of Carbon Nanostructures. Adv Mater. 30(17):e1705630.

5. Balachandran A, Sreenilayam SP, Madanan K, Thomas S, Brabazon D. (2022). Nanoparticle production via laser ablation synthesis in solution method and printed electronic application - A brief review. Results in Engineering. 16:100646.

6. Torrisi L, Silipigni L, Torrisi A, Cutroneo M. (2024). Luminescence in laser-generated biocompatible functionalized Carbon dots. Optics and Laser Technology.

7. Torrisi L, Silipigni L, Restuccia N, Cuzzocrea S, Cutroneo M, Barreca F, et al. (2018). Laser-generated bismuth nanoparticles for applications in imaging and radiotherapy. Journal of Physics and Chemistry of Solids. 119:62-70.

8. Torrisi L, Torrisi A. (2020). Ni, Ti, and NiTi laser ablation in vacuum and in water to deposit thin films or to generate nanoparticles in solution. Contributions to Plasma Physics. 61(1):e202000070.

9. LeCroy GE, Yang ST, Yang F, Liu Y, Fernando KAS, Bunker CE, et al. (2016). Functionalized carbon nanoparticles: Syntheses and applications in optical bioimaging and energy conversion. Coordination Chemistry Reviews. 320-321:66-81.

10. Torrisi L, Torrisi A, Cutroneo M. (2024). Intense CW laser to synthetize luminescent solution of Carbon dots. Fullerenes, Nanotubes and Carbon nano structures.

11. Fréjaville T, Carcaillet C, Curt T. (2013). Calibration of charcoal production from trees biomass for soil charcoal analyses in subalpine Ecosystems. Quaternary International. 289:16-23.

12. Tumuluru JS, Hess JR, Boardman RD, Wright CT,. Westover TL. (2012). Formulation, Pretreatment, and Densification Options to Improve Biomass Specifications for Co-Firing High Percentages with Coal. Industrial Biotechnology. 8(3):113-132.

13. Siemons RV, Baaijens L. (2012). An Innovative Carbonisation Retort: Technology and Environmental Impact. Termotehnika XXXVIII. 2:131-138.

14. Acqua-calc.com, Density of Charcoal (material), actual website 2024: Density of Charcoal in 285 units of density (aqua-calc.com)

15. Ganjoo R, Sharma S, Kumar A, Daouda MMA. Chapter 1: Activated Carbon: Fundamentals, Classification, and Properties, Special Collection: 2023 ebook collection, 2023. DOI: https://doi.org/10.1039/BK9781839169861-00001

16. My Engineering tool, database. Actual website 2024: Thermal Conductivity : chart of 300+ common materials (myengineeringtools.com)

17. Kurniati M, Nurhayati D, Maddu A. (2017). Study of Structural and Electrical Conductivity of Sugarcane Bagasse-Carbon with Hydrothermal Carbonization. IOP Conf. Series: Earth and Environmental Science. 58:012049.

18. de Abreu Neto R, de Assis AA, Ballarin AW, Hein PRG. (2018). Dynamic Hardness of Charcoal Varies According to the Final Temperature of Carbonization. Energy Fuels. 32(9):9659-9665.

19. Phosphate-buffered saline (PBS) recipe. CSH Protocol. Actual website 2024: Phosphate-buffered saline (PBS) (cshlp.org)

20. Sigma-Aldrich, phosphate buffer saline. Actual website 2024: https://www.sigmaaldrich.com/IT/it/substance/phosphatebufferedsaline1234598765

21. El-Eswed B. (2015). Effect of basicity and hydrophobicity of amines on their adsorption onto charcoal. Desalination and Water Treatment.

22. Chen ZW, Hsieh TH, Liu CP. (2022). Production of carbon dots by pulsed laser ablation: Precursors and photo-oxidase properties. J Chin Chem Soc. 69(1):193-199.

23. Cao L, Zan M, Chen F, Kou X, Liu Y, Wang P, et al. (2022). Formation mechanism of carbon dots: From chemical structures to fluorescent behaviors. Carbon. 194:42-51.

ISSN: 2767-0171

24. Li P, Xue S, Sun L, Zong X, An L, Qu D, et al. (2022). Formation and fluorescent mechanism of red emissive carbon dots from o-phenylenediamine and catechol system. Science & Applications 11:298.

25. Wu L, Cai X, Nelson K, Xing W, Xia J, Zhang R, et al. (2013). Agreen synthesis of carbon nanoparticles from honey and their use in real-time photoacoustic Imaging. Nano Res. 6:312–325.

26. Thambiraj S, Ravi Shankaran D. (2016). Green synthesis of highly fluorescent carbon quantum dots from sugarcane bagasse pulp. Appl Surf Sci. 390:435-443.

27. Yogesh GK, Shuaib EP, Priya AK, Rohini P, Anandhan SV, Krishnan UM, et al. (2021). Synthesis of water-soluble fluorescent carbon nanoparticles (CNPs) from nanosecond pulsed Laser ablation in ethanol. Optics and Laser Technology. 135:106717.

28. Yeh TF, Huang WL, Chung CJ, Chiang IT, Chen LC, Chang HY, et al. (2016). Elucidating quantum confinement in graphene oxide dots based on excitation-wavelength-independent photoluminescence. J Phys Chem Lett. 7(11):2087-2092.

29. Liu Y, Kilby P, Frankcombe TJ, Schmidt TW. (2019). Electronic transitions of molecules: vibrating Lewis structures. Chem Sci. 10(28):6809-6814.

30. Ozyurt D, Al Kobaisi M, Hocking RK, Fox B. (2023). Properties, synthesis, and applications of carbon dots: A review. Carbon Trends. 12:100276.

31. Shuaib EP, Shafi PM, Yogesh GK, Bose AC, Sastikumar D. (2019). Carbon nanoparticles synthesized by laser ablation of coconut shell charcoal in liquids for glucose sensing applications. Mater Res Express. 6:115610.

32. Alkian I, Sutanto H, Hadiyanto. (2022). Quantum yield optimization of carbon dots using response surface methodology and its application as control of Fe3+ion levels in drinking water. Mater Res Express. 9(1):015702.

33. Salinas-Castillo A, Ariza-Avidad M, Pritz C, Camprubí-Robles M, Fernández B, Ruedas-Rama MJ, et al. (2013). Carbon dots for copper detection with down and upconversion fluorescent properties as excitation sources. Chem Commun. 49(11):1103-1105.

34. Yuan C, Liu B, Liu F, Han MY, Zhang Z. (2014). Fluorescence "turn on" detection of mercuric ion based on bis(dithiocarbamato)copper(II) complex functionalized carbon nanodots. Anal Chem. 86(2):1123-1130.

35. Gao X, Ding C, Zhu A, Tian Y. (2014). Carbon-dot-based ratiometric fluorescent probe for imaging and biosensing of superoxide anion in live cells. Anal Chem. 86(14):7071-7078.

36. Wang R, Li G, Dong Y, Chi Y, Chen G. (2013). Carbon quantum dot-functionalized aerogels for NO2 gas sensing. Anal Chem. 85(17):8065-8069.

37. Yu C, Li X, Zeng F, Zheng F, Wu S. (2013). Carbon-dot-based ratiometric fluorescent sensor for detecting hydrogen sulfide in aqueous media and inside live cells. Chem Commun (Camb). 49(4):403-405.

38. Zhang J, Yu SH. (2016). Carbon dots: large-scale synthesis, sensing and bioimaging. Materials Today. 19(7):382-393.

39. Song Y, Shi W, Chen W, Lia X, Ma H. (2012). Fluorescent carbon nanodots conjugated with folic acid for distinguishing folate-receptor-positive cancer cells from normal cells. J Mater Chem. 22(25):12568-12573.

40. Lee CH, Rajendran R, Jeong MS, Ko HY, Joo JY, Cho S, et al. (2013). Bioimaging of targeting cancers using aptamer-conjugated carbon nanodots. Chem Commun. 49(58):6543-6545.

Citation: Torrisi L, et al. (2024). Carbon Dots Synthetization by Intense CW Laser at 450 nm. Nanoparticle. 5(1):14.

DOI: https://doi.org/10.35702/nano.10014